SINGLE-SHOT MULTISPECTRAL IMAGE ACQUISITION FOR LOW-ALTITUDE REMOTE SENSING USING LIGHT DIFFRACTION TECHNIQUES

Carlos Iturrino[1,2]*,Fernando X. Arias*[1,2]*, Heidy Sierra*[1,2]*, Emmanuel Arzuaga*[1,2,3]

1. Laboratory for Applied Remote Sensing, Imaging and Photonics
2. Department of Electrical and Computer Engineering
3. Department of Computer Science and Engineering
University of Puerto Rico Mayaguez

ABSTRACT

Multispectral imaging devices currently being used in a variety of applications typically follow opto-mechanical designs. These designs often present the disadvantage of a bulky and heavy construction, limiting their applicability in new low-altitude remote sensing applications deployed on acquisition systems with constrained weight and dimension requirements. This paper presents the design and construction of a simple optical system based on a transmission grating and a lightweight commercial camera for snapshot multispectral image acquisition. The system can be mounted on a small drone for low-altitude aerial remote sensing, and is capable of separating the spectral information from the spatial scene and generating multispectral HD images and 4K videos. In addition, we propose a fast algorithm for recovering multispectral scenes from their respective acquired spectral projections. Experimental results show similarity of the compared waveforms, and that the maximum peak of the reconstructed wavelength varies up to 13nm from reference spectroradiometer data.

Index Terms— Multispectral Imaging, Adaptive Optics, Relay Lens, Transmission Grating, Drone, Reconstruction Algorithm, Convolution

1. INTRODUCTION

Multispectral Imaging enables the non-invasive acquisition of images of a given target in a large number of individual spectral bands, and has numerous current applications such as crop field monitoring, ocean and earth topography, and biomedical imaging [1] [2]. In oceanography applications, spectral instrument readings are used to measure ocean color products. These products commonly include harmful algae blooms (HABs), oil spills and chlorophyll concentration. The main limitation of established spectral measuring instruments is that they have low spatial resolution. An example of which is LANDSAT 8, which has a spatial resolution of 30m [3]. The spectral irradiance of a given target is unique for every material. Spectrally-resolved measurements enable an user to identify and classify targets based on the intensity of each spectral band. Currently, there are various techniques for capturing multispectral images including: Whisk Broom [4], Push Broom [5] and Computer Tomography Imaging Spectrometer (**CTIS**)[6, 7]. While the Whisk broom and Push Broom techniques require opto-mechanical scanning of the image plane (which is costly, time consuming, and can increase device cost and dimensions), CTIS only requires a single snapshot and minimum opto-mechanical components. This can be useful and more efficient when capturing transient phenomena. Commercially available multispectral imaging systems tend to be costly, with starting prices in the range of $\$8{,}000 - \$100{,}000$ [8]. However, the use of CTIS introduces the requirement of specialized algorithms for recovering the spectrally-resolved images. The information provided by such a device is thus dependent on the camera's resolution and its native spectral sensitivity.

The main contribution of this work is to present the results of building a low-cost, lightweight multispectral imager for UAV applications, together with CTIS-based algorithms to acquire spectral image data. The rest of the paper is organized as follows: section 3 describes the operation fundamentals of a CTIS device, section 3.1 describes the proposed fast convolutional approach for CTIS image recovery and section 4 describes the design and construction of the optical device. Finally, section 5 presents our results, compared to commodity spectral measurement devices.

2. RELATED WORK

Previous work has shown that unmodified commercial RGB cameras can successfully capture multispectral images using a CTIS-based approach [6], thus preserving the advantages introduced by CTIS: avoiding opto-mechanical components, a simple optical path, and snapshot acquisition of the entire scene. Alternatively, [8] presents a compact single-shot hyperspectral imaging method using a conventional DSLR camera equipped with an ordinary refractive prism. In this approach, the computational imaging method recovers the

spectral information of a scene from edge dispersion, with the added constraint of a time-consuming recovery algorithm that limits applications with imaging speed requirements. In addition, a novel 3D hyperspectral imaging system based on integration of compressive sensing and light-field imaging was proposed [7]. The basic idea of this work is to use the recorded light rays to compute a final image, called a synthetic image. So the light-field computation develops hyperspectral imaging system using compressive sensing. They combine the directional information with the spatial information supplied by the sub-aperture images which enables the reconstruction of a hyperspectral image in a new direction [9]. Finally, low-altitude hyperspectral observation systems using aerial observation with unmanned aerial vehicles (UAVs) have advantages over satellite systems with respect to frequency, accuracy, and spatial resolution [10]. These considerations make spectral imaging via a UAV an attractive solution for localized remote sensing applications[11, 12]. The currently exist commercial alternatives for the specific case of multispectral UAV imaging [13]. However, they typically present a multiple photo-detectors imagers, adding complexity to their design.

3. CTIS RECONSTRUCTION THEORY

The CTIS image recovery problem is formulated as a generalized linear continuous to discrete system [14] described by Equation 1. Where g is the data acquired by the sensor, H is the transformation and f is the hyperspectral data cube.

$$g_m = \int_s f(r) h_m(r) dr \tag{1}$$

Let f be a multi or hyperspectral image represented as a rank-3 discrete tensor signal where X Y Λ are integers representing the spatial and spectral dimensionality. Conversely, let Z_X, Z_Y and Z_Λ be the set of $\{0, 1, \ldots, X-1\}$, $\{0, 1, \ldots, Y-1\}$ and $\{0, 1, \ldots, \Lambda - 1\}$ respectively. $Z_{XY\Lambda}$ be the set of $\{1, 2, \ldots, 255\}$. The linear mapping of f is seen in Equation 2.

$$\begin{aligned} f &: \mathbb{Z}_X \times \mathbb{Z}_Y \times \mathbb{Z}_\Lambda \to \mathbb{Z}_{XY\Lambda} \\ (x, y, \lambda) &\mapsto f(x, y, \lambda) = v \end{aligned} \tag{2}$$

Let g be an RGB image represented as a rank-2 discrete tensor signal where M and N be integers representing the signal dimensionality and Z_M and Z_N be the set of $\{0, 1, \ldots, M-1\}$, $\{0, 1, \ldots, N-1\}$ respectively. Z_{MN} be the set of $\{1, 2, \ldots, 255\}$. The linear mapping of g is seen in Equation 3.

$$\begin{aligned} g &: \mathbb{Z}_M \times \mathbb{Z}_N \to \mathbb{Z}_{MN} \\ (m, n) &\mapsto g(m, n) = c \end{aligned} \tag{3}$$

The definition of H is seen in Equation 4. H is a linear operator acting on f to produce g which is defined in Equation 3. g is the spatial and spectral information in the image plane acquired by the camera:

$$\begin{aligned} H &: l^2(Z_N \times Z_N \times Z_N) \to l^2(Z_N \times Z_N) \\ f &\mapsto H\{f\} = g \end{aligned} \tag{4}$$

where $I_{x\times y}$ is identity matrix and $\mathbf{a}_{(kp+1)\times k}$ is seen in Equation 5. k is the number of spectral bands and p the number of projections.

$$H = \{H \in \mathbb{R} : H = I_{x\times y} \otimes \mathbf{a}_{(kp+1)\times k}\} \tag{5}$$

$$a_{(kp+1)\times k} = \begin{bmatrix} J_{k\times k} & J_{k\times k} & U_k & I_{k\times k} & I_{k\times k} \end{bmatrix}^T \tag{6}$$

3.1. Convolutional Reconstruction of CTIS Images

The proposed convolutional reconstruction algorithm recovers multispectral CTIS images through the convolution between the image plane $g[n_1, n_2]$ and the impulse response of the given spectral bands $h[n_1, n_2]$. In other words, the convolution between the image containing the spatial and spectral information and the artificial image created with an impulse in the location of the projection of each spectral band. This operation produces a recovered multispectral image with the intensity of each spectral band. The 2-dimensional convolution operation is presented in Equation 7.

$$F[n_1, n_2] = \sum_{k_1 k_2} g[k_1, k_2] h[n_1 - k_1, n_2 - k_2] \tag{7}$$

Thus, the recovery of the spectral cube using a convolution operation can be formulated as follows. Let h be the linear operator on g, as seen in Equation 8. This operation is equivalent to a convolution, as shown in Equation 9:

$$\begin{aligned} h &: l^2(Z_N \times Z_N) \to l^2(Z_N \times Z_N) \\ g &\mapsto h\{g\} = F \end{aligned} \tag{8}$$

$$\begin{aligned} * &: l^2(Z_N) \to l^2(Z_N) \\ (g, h) &\mapsto *\{(g, h)\} \triangleq g * h = F \end{aligned} \tag{9}$$

where h and g are as presented in Equations 10 and 11. The elements $p_1\ p_2\ p_3\ p_4\ p_0$ are the projections of the target image, including the order zero. The 2-dimensional convolution is seen in Equation 12 where S is $p_1 + p_2 + p_3 + p_4 + p_0$ constitute the intensity image in a given spectral band λ_k.

$$h[n_1, n_2] = \begin{bmatrix} 0_{1,1} & \ldots & 0_{1,j} & 1_{1,j+1} & 0_{1,j+2} & \ldots & 0_{1,n_2} \\ \vdots & & \vdots & \vdots & \vdots & & \vdots \\ 0_{i,1} & \ldots & 0_{i,j} & 0_{i,j+1} & 0_{i,j+2} & \ldots & 0_{i,n_2} \\ 1_{i+1,1} & \ldots & 0_{i+1,j} & 1_{i+1,j+1} & 0_{i+1,j+2} & \ldots & 1_{i+1,n_2} \\ 0_{i+2,1} & \ldots & 0_{i+2,j} & 0_{i+2,j+1} & 0_{i+2,j+2} & \ldots & 0_{i+2,n_2} \\ \vdots & & \vdots & \vdots & \vdots & & \vdots \\ 0_{n_1,1} & \ldots & 0_{n_1,j} & 1_{n_1,j+1} & 0_{n_1,j+2} & \ldots & 0_{n_1,n_2} \end{bmatrix} \tag{10}$$

$$g[n_1, n_2] = \begin{bmatrix} \mathbf{0} & \mathbf{p}_1 & \mathbf{0} \\ \mathbf{p}_2 & \mathbf{p}_0 & \mathbf{p}_4 \\ \mathbf{0} & \mathbf{p}_3 & \mathbf{0} \end{bmatrix} \tag{11}$$

$$F[N_1, N_2] = \begin{bmatrix} \mathbf{0} & \mathbf{0} & \mathbf{p_1} & \mathbf{0} & \mathbf{0} \\ \mathbf{0} & \mathbf{p_1 + p_2} & \mathbf{p_0 + p_1} & \mathbf{p_1 + p_4} & \mathbf{0} \\ \mathbf{p_2} & \mathbf{p_2 + p_0} & \mathbf{S} & \mathbf{p_4 + p_0} & \mathbf{p_4} \\ \mathbf{0} & \mathbf{p_2 + p_3} & \mathbf{p_0 + p_3} & \mathbf{p_4 + p_3} & \mathbf{0} \\ \mathbf{0} & \mathbf{0} & \mathbf{p_3} & \mathbf{0} & \mathbf{0} \end{bmatrix} \tag{12}$$

4. CTIS-BASED SPECTRAL IMAGING DEVICE

With the objective of designing a low-cost, portable multispectral imaging device, our design is based on a GoPro Hero 6 camera. This camera was further augmented using a fabricated attachment that enables the acquisition of spatio-spectral CTIS images. This attachment mainly consists of an imaging lens, an iris, a collimating lens and a diffraction grating. For reference, an optical diagram of the attachment is shown in Figure 1, and the complete attachment in Figure 2.

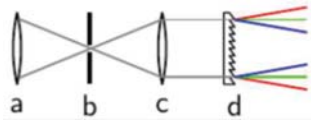

Fig. 1. Diagram of optical system

Fig. 2. Diagram of optical system

Once the optical path and core components for the attachment are determined, the tubing system in Figure 2 was constructed. The attachment was constructed using ⌀2" lenses with a 40mm focal length for the imaging and collimating lenses, ⌀2" adjustable length threaded tube and a ring-actuated ⌀1mm - ⌀25mm adjustable iris diaphragm from the Thorlabs SM2 family. Because the system is developed for low altitude scenarios, this allows the acquisition of .5m to 10m of spatial information. This is done to complement loss of spatial resolution from satellite data. A ⌀2" lens with low focal length can be mounted on a drone camera. For the case of CTIS imaging, there exists a trade-off between the spatial information acquired and the overlapping between spectral bands in the spectral projections in the image plane. If the aperture is maximally opened, spectral bands overlap, which is detrimental to the spectral resolution of recovered images. Alternatively, a minimal aperture results in single pixel measurements with very detailed spectral information. Thus, the system aperture is set that the camera captures 92mm for every meter of distance. Thus if, for instance, the drone flies at 10m, it can capture .920 m of spatial information without sacrificing spectral information.

Fig. 3. Prototype system using a GoPro Karma Drone with a Hero 6 camera and the spectral imaging filter.

A Rainbow Symphony film transmission grating with 532 lines/mm is used on the setup. This allows the camera to capture the first order projection of the scene in the visible range. In order to capture these projections in two dimensions,two gratings were superimposed with a 90 degree rotational offset.

The calibration procedure consists of determining the position of each spectral band in the image plane with respect to the zero-order image. For this purpose, a Mercury-Argon lamp with known wavelengths (435.833nm, 546.074nm, and 696.543nm) was used. This procedure is performed with a 1mm aperture, and the distance from the zero order to each projection is measured. From these distance measurements, the rest of possible wavelengths is interpolated.

5. RESULTS

Following calibration, experiments were performed by capturing an image with both 2 colors and multiple colors, and comparing the recovered spectral response with a calibrated SOC700 hyperspectral camera as ground truth. Figure 4 presents and compares the reconstruction results using the proposed convolutional approach. It adequately preserves spatial resolution from a distance of 1m and a field of view of 4.563 cm. In addition, Figure 5 shows the comparison of spectral waveforms of different colors with the measurements from a GER 1500 spectroradiometer, used as ground truth. With a reconstruction time of 56 seconds per data cube, the convolutional approach was able to reconstruct 8

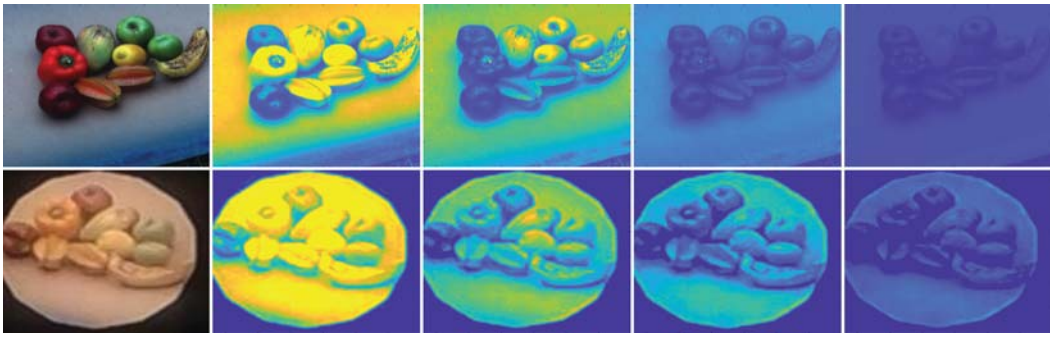

Fig. 4. Comparison of images acquired using a SOC700 hyperspectral camera (top row) and the proposed CTIS instrument (bottom row). Columns, from left to right: RGB composite, 600nm band, 520nm band, 460nm band, 400nm band.

Table 1. MSE CTIS and GER1500 and SOC700

Color	GER 1500	SOC 700
Red 1	0.0586	0.0190
Red 2	0.0335	0.0338
Orange	0.0218	0.0416
Yellow	0.0123	0.0230
Green 1	0.0637	0.0146
Green 2	0.0235	0.0304
Blue 1	0.0433	0.1057
Blue 2	0.0535	0.0385

Table 2. Camera Parameters

Parameter	Values
Spectral Range	400nm-600nm
Resolution between bands	10nm
Spectral Resolution	42nm
Spatial Resolution	92mm per m
AFOV	3.42

multispectral data cubes making a total of 7 minutes and 28 seconds. Each one with 41 spectral bands from 300 nm to 700 nm. Results the comparison between the spectral data of the spectroradiometer and the camera have similar waveforms.

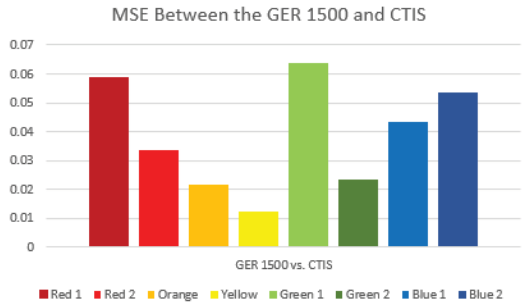

Fig. 5. MSE graph comparing the GER 1500 spectroradiometer with the CTIS instrument

6. CONCLUSION

A low-cost multispectral camera using simple optical components and an unmodified consumer camera with a spectral resolution of 60nm was developed. In addition, a convolutional approach for CTIS image recovery was proposed, which produced fast and accurate results verified with calibrated devices as ground truth information. Our results indicate little to no discernible loss in both spatial and spectral resolution. The fast CTIS reconstruction time of this approach enables its use in applications with dynamic scenes and/or transient phenomena.

Future work includes the integration of a more complex optical design, and further optimizing the convolutional recovery algorithm for enhanced spectral resolution. In addition, the use of a camera with a wider spectral sensitivity can provide additional spectral data, and increase its viability for other applications.

7. ACKNOWLEDGEMENTS

This study is supported in part and monitored by NOAA-CESSRST under the Cooperative Agreement # NA16SEC4810008. F.A. is supported by a scholarship grant from the Instituto para la Formacion y Aprovechamiento de Recursos Humanos (IFARHU) office of the government of the Republic of Panama. This work is supported in part by the Laboratory for Applied Remote Sensing, Imaging and Photonics (LARSIP) at the University of Puerto Rico Mayaguez.

8. REFERENCES

[1] Anton Vrieling, "Satellite remote sensing for water erosion assessment: A review," *CATENA.*, vol. 65, 2006.

[2] A. H. S. Solberg, "Remote sensing of ocean oil-spill

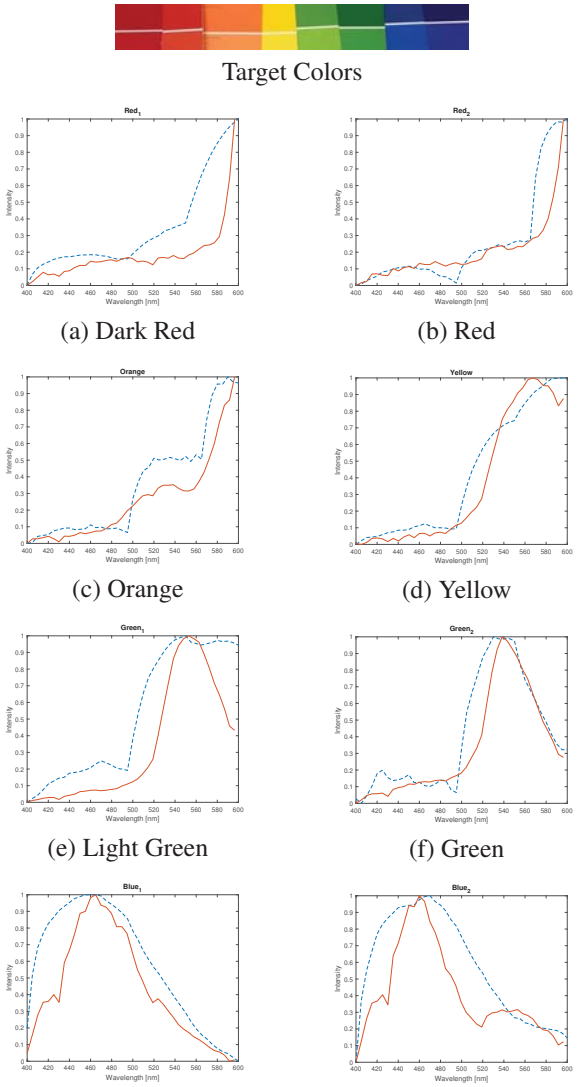

(a) Dark Red (b) Red

(c) Orange (d) Yellow

(e) Light Green (f) Green

(g) Blue (h) Dark Blue

Fig. 6. Comparison of the camera with spectroradiometer: (a) From left to Right:Dark Red, Red, Orange, Yellow, Light Green, Green, Blue, Dark Blue.

pollution," *Proceedings of the IEEE*, vol. 100, no. 10, pp. 2931–2945, 2012.

[3] Jeffrey G. Masek, Michael P. Taylor, and Laura Rocchio, "Nasa. landsat science. landsat 8 overview.," .

[4] J. E. Fowler, "Compressive pushbroom and whiskbroom sensing for hyperspectral remote-sensing imaging," in *2014 IEEE International Conference on Image Processing (ICIP)*, Oct 2014, pp. 684–688.

[5] J. P. Kerekes and J. R. Schott, "Hyperspectral imaging systems," in *Hyperspectral Data Exploitation: Theory and Applications*, The editor, Ed., chapter 12, pp. 19–45. C.-I. Chang, Hoboken, NJ: John Wiley & Sons, Inc., 2007.

[6] Rafael Babel, Michael Kudenov, and Michael Wimmer, "Practical Spectral Photography.," *EUROGRAPHICS*, vol. 31, no. 2, 2012.

[7] Yitzhak August, Chaim Vachman, Yair Rivenson, and Adrian Stern, "Compressive hyperspectral imaging by random separable projections in both the spatial and the spectral domains," 2013.

[8] Seung-Hwan Baek, Incheol Kim, Diego Gutierrez, and Min H. Kim, "Compact single-shot hyperspectral imaging using a prism," *ACM Trans. Graph. 36, 6, Article 217 (November 2017), 12 pages*, 2017.

[9] King Wai, Chiu Lai, Ning Xi, Hongzhi Chen, Liangliang Chen, , and Bo Song, "Development of 3d hyperspectral camera using compressive sensing," *IEEE*, 2012.

[10] Kuniaki Uto, Haruyuki Seki, Genya Saito, Yukio Kosugi, and Teruhisa Komatsu, "Development of a low-cost, lightweight hyperspectral imaging system based on a polygon mirror and compact spectrometers.," *"IEEE"*, vol. "09", no. "02", "2016".

[11] Richard H.Becker, Michael Sayers, Dustin Dehm, Robert Shuchman, Kaydian Quintero, Karl Bosse, and Reid Sawtell, "Unmanned aerial system based spectroradiometer for monitoring harmful algal blooms: A new paradigm in water quality monitoring," *Journal of Great Lakes Research*, 2019.

[12] H. Saaria, A. Akujrvia, C. Holmlunda, H. Ojanena, J. Kaivosojab, A. Nissinenb, and O. Niemelinenb, "Visible, very near ir and short wave ir hyperspectral drone imaging system for agriculture and natural water applications," *Frontiers in Spectral imaging and 3D Technologies for Geospatial Solutions,*, vol. XLII-3/W3, pp. 2527, 2017.

[13] Kathrin Maier, "Direct multispectral photogrammetry for uav-based snow depth measurements," 2019.

[14] William R. Johnson, Daniel W. Wilson, , and Greg Bearman, "Spatialspectral modulating snapshot hyperspectral imager.," *Applied Optics,*, vol. 45, pp. 1868–1908, 2016.